NASA/TM—2006-214268 AIAA–2006–0261

Dynamic Wind-Tunnel Testing of a Sub-Scale Iced Business Jet

Sam Lee
QSS Group, Inc., Cleveland, Ohio

Billy P. Barnhart
Bihrle Applied Research, Inc., Jericho, New York

Thomas P. Ratvasky
Glenn Research Center, Cleveland, Ohio

Edward Dickes
Bihrle Applied Research, Inc., Jericho, New York

Michael Thacker
Cessna Aircraft Company, Wichita, Kansas

May 2006

NASA STI Program . . . in Profile

Since its founding, NASA has been dedicated to the advancement of aeronautics and space science. The NASA Scientific and Technical Information (STI) program plays a key part in helping NASA maintain this important role.

The NASA STI Program operates under the auspices of the Agency Chief Information Officer. It collects, organizes, provides for archiving, and disseminates NASA's STI. The NASA STI program provides access to the NASA Aeronautics and Space Database and its public interface, the NASA Technical Reports Server, thus providing one of the largest collections of aeronautical and space science STI in the world. Results are published in both non-NASA channels and by NASA in the NASA STI Report Series, which includes the following report types:

- TECHNICAL PUBLICATION. Reports of completed research or a major significant phase of research that present the results of NASA programs and include extensive data or theoretical analysis. Includes compilations of significant scientific and technical data and information deemed to be of continuing reference value. NASA counterpart of peer-reviewed formal professional papers but has less stringent limitations on manuscript length and extent of graphic presentations.

- TECHNICAL MEMORANDUM. Scientific and technical findings that are preliminary or of specialized interest, e.g., quick release reports, working papers, and bibliographies that contain minimal annotation. Does not contain extensive analysis.

- CONTRACTOR REPORT. Scientific and technical findings by NASA-sponsored contractors and grantees.

- CONFERENCE PUBLICATION. Collected papers from scientific and technical conferences, symposia, seminars, or other meetings sponsored or cosponsored by NASA.

- SPECIAL PUBLICATION. Scientific, technical, or historical information from NASA programs, projects, and missions, often concerned with subjects having substantial public interest.

- TECHNICAL TRANSLATION. English-language translations of foreign scientific and technical material pertinent to NASA's mission.

Specialized services also include creating custom thesauri, building customized databases, organizing and publishing research results.

For more information about the NASA STI program, see the following:

- Access the NASA STI program home page at *http://www.sti.nasa.gov*

- E-mail your question via the Internet to *help@sti.nasa.gov*

- Fax your question to the NASA STI Help Desk at 301–621–0134

- Telephone the NASA STI Help Desk at 301–621–0390

- Write to:
  NASA STI Help Desk
  NASA Center for AeroSpace Information
  7121 Standard Drive
  Hanover, MD 21076–1320

NASA/TM—2006-214268 AIAA–2006–0261

Dynamic Wind-Tunnel Testing of a Sub-Scale Iced Business Jet

Sam Lee
QSS Group, Inc., Cleveland, Ohio

Billy P. Barnhart
Bihrle Applied Research, Inc., Jericho, New York

Thomas P. Ratvasky
Glenn Research Center, Cleveland, Ohio

Edward Dickes
Bihrle Applied Research, Inc., Jericho, New York

Michael Thacker
Cessna Aircraft Company, Wichita, Kansas

Prepared for the
44th Aerospace Sciences Meeting and Exhibit
sponsored by the American Institute of Aeronautics and Astronautics
Reno, Nevada, January 9–12, 2006

National Aeronautics and
Space Administration

Glenn Research Center
Cleveland, Ohio 44135

May 2006

Level of Review: This material has been technically reviewed by technical management.

Available from

NASA Center for Aerospace Information
7121 Standard Drive
Hanover, MD 21076–1320

National Technical Information Service
5285 Port Royal Road
Springfield, VA 22161

Available electronically at http://gltrs.grc.nasa.gov

Dynamic Wind-Tunnel Testing of a Sub-Scale Iced Business Jet

Sam Lee
QSS Group, Inc.
Cleveland, Ohio 44135

Billy P. Barnhart
Bihrle Applied Research, Inc.
Jericho, New York 11753

Thomas P. Ratvasky
National Aeronautics and Space Administration
Glenn Research Center
Cleveland, Ohio 44135

Edward Dickes
Bihrle Applied Research, Inc.
Jericho, New York 11753

Michael Thacker
Cessna Aircraft Company
Wichita, Kansas 67218

The effect of ice accretion on a 1/12-scale complete aircraft model of a business jet was studied in a rotary-balance wind tunnel. Three types of ice accretions were considered: ice protection system failure shape, pre-activation roughness, and runback shapes that form downstream of the thermal ice protection system. The results were compared with those from a 1/12-scale semi-span wing of the same aircraft at similar Reynolds number. The data showed that the full aircraft and the semi-span wing models showed similar characteristics, especially post stall behavior under iced configuration. However, there were also some discrepancies, such as the magnitude in the reductions in the maximum lift coefficient. Most of the ice-induced effects were limited to longitudinal forces. Rotational and forced oscillation studies showed that the effects of ice on lateral forces were relatively minor.

Nomenclature

b	=	aircraft span
C_l	=	aircraft rolling coefficient
C_L	=	aircraft lift coefficient
$C_{L,max}$	=	aircraft maximum lift coefficient
LWC	=	liquid water content
$m.a.c.$	=	mean aerodynamic chord
OAT	=	outside air temperature
p	=	aircraft roll rate
q_∞	=	freestream dynamic pressure
V	=	airspeed
α	=	aircraft angle of attack
δe	=	elevator deflection angle
δf	=	flap deflection angle
Ω	=	rotational rate about the velocity vector

I. Introduction

AN icing-effects flight simulation model for a typical business jet is currently being developed by NASA, Cessna, and Bihrle Applied Research. The simulation model will be implemented into a flight training device for pilot evaluation prior to flight testing of an ice shape and for pilot training. The hardware to be used is from an icing flight simulation demonstrator for a turbo-prop commuter aircraft that was developed under a previous effort.[1,2,3]

The flight simulation model to be used in the flight training device was developed by testing a 1/12-scale complete aircraft model in a rotary-balance-equipped vertical-flow wind tunnel. Three types of ice accretions were considered: ice protection system failure shape, pre-activation roughness, and runback shapes that form downstream of the thermal ice protection system. Because of the significant reduction in both the geometry and the Reynolds number, the scaling relationship between the full-scale aircraft and the subscale model was investigated and reported.[4] Full-scale, 5/12-scale, and 1/12-scale semi-span wing sections were tested at various Reynolds numbers with and without ice shapes. The full-scale and 5/12-scale models were tested in the Langley Full-Scale Tunnel (LFST) in Hampton, VA. The 1/12-scale model was tested in the University of Illinois Subsonic Tunnel in Urbana, IL. The results showed that the geometrically-scaled failure shape was insensitive to Reynolds number effects and did not require additional scaling. The pre-activation roughness could be scaled to 1/12 of full scale by choosing appropriate grit height. The runback shape exhibited significant Reynolds number variation and required significant adjustment of the data to correlate to full-scale data.

The data collected from a 1/12-scale model of the complete aircraft were used as the primary basis for developing a new aircraft simulation for the iced conditions. Results from the tests of partial wing panels of this aircraft in three different scales were used to modify the results of the complete airplane tests, as required, to model the full-scale airplane characteristics under iced conditions.

II. Experimental Methods

The test was conducted in the Bihrle Applied Research Large Amplitude Multi-Purpose (LAMP) facility in Neuberg a.d. Donau, Germany. The LAMP facility consists of an open circuit, 78-ft high, low-speed vertical wind tunnel having a circular cross section. A constant 10-ft diameter circular cross-section test area is used for all static, rotational, forced oscillation, pressure, and flow visualization tests. Within this test section, the velocity can be set at any desired speed, up to a maximum of 120 ft/sec. Model installation and configuration modifications are conveniently performed in the area outside the tunnel test section since the entire test rig, including the model, can be quickly moved in and out of the tunnel on a motorized traveling beam. A six-component strain-gauge balance, affixed to the end of the sting and mounted inside the model, is used to measure the six forces and moments acting along and about the model body axis. A control panel located outside the tunnel test section is used to activate the motors on the rig, which position the model to the desired attitude. Electrical currents from the balance and the motors on the rig are conducted through slip rings. Shown in Fig. 1 is the model mounted in the test section.

As stated previously, the model tested was a 1/12-scale model of a typical business jet. It was constructed of fiberglass, balsa, and plywood. A metal model had been provided to obtain molds for construction of this light-weight dynamic model. The model was equipped with moveable control surfaces (aileron, rudder, elevator, and flaps). The ice shapes chosen for testing consisted of the following:

- Ice protection system failure
- Pre-activation roughness
- Runback ice shapes that form downstream of thermal anti-ice system

The geometry of failure shape and pre-activation roughness on the wing ice protection system was obtained from LEWICE[5] calculations using the following conditions:

Table 1. Icing conditions for failure and pre-activation roughness.

Ice Shape	Aircraft α	V (KCAS)	LWC (g/m^3)	MVD (μm)	OAT (F)
22.5-min. failure	3.08 deg	160	0.6	15	14
2 min. roughness	3.08 deg	160	0.3	15	-4

Figure 1. Business jet aircraft model in LAMP test section.

Because the pre-activation shape did not have any significant ice thickness, it was simulated using only roughness. The runback shape used for the full-scale aircraft was typical of that encountered during natural and tanker icing encounters. All three ice shapes were modified from the full-scale version for the 1/12-scale complete aircraft test using the results from the scaling studies.

The failure shape was geometrically scaled from the full-scale version. The full-scale version was covered with 40-grit roughness in order to simulate ice roughness. However, the scaling studies showed that this was not necessary on the 1/12-scale shape. The full-scale pre-activation roughness was simulated with 40-grit sandpaper. However, for the 1/12-scale model, 40-grit silicon carbide grit sprinkled on double-sticky tape was used instead. The runback shape behind the wing ice protection system was replaced with an equivalent shape (a simpler geometry providing equivalent aerodynamic degradation) consisting of piano wire on the upper surface and square balsa-wood stock on the lower surface. In addition to these wing shapes, ice shape simulations were placed on other parts of the aircraft as well. This will be discussed in more detail below.

1. Failure ice shape configuration.

The failure shape configuration consisted of 1/12-scale failure shape on the wing ice protection system (using conditions shown in Table 1). The tail ice protection system was assumed to be operational, and inter-cycle roughness (40-grit) was used on protected tail surfaces. On the unprotected portion of the wing and tail, LEWICE generated ice shapes (using the same condition shown in Table 1, but for 45-minute) were used. On this aircraft, the horizontal stabilizer is protected with a pneumatic boot and the vertical stabilizer is not protected. All of the LEWICE generated ice shapes were fabricated using stereo lithography. The failure shape configuration on the wing and tail are shown in Figs. 2a and 2b, respectively.

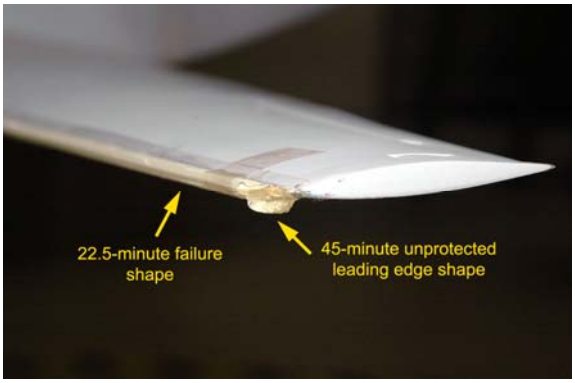

Fig. 2a) Wing

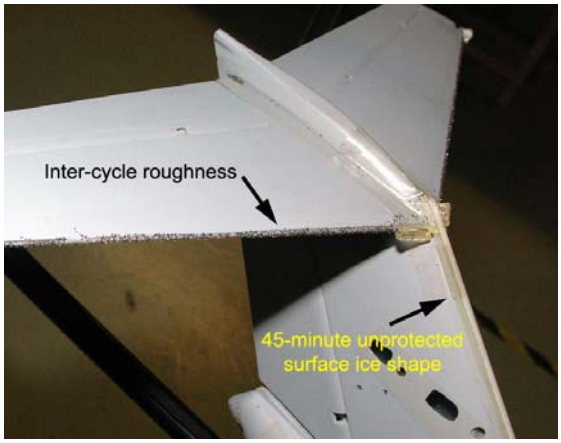

Fig. 2b) Tail

Figure 2. Failure shape configuration.

2. Pre-activation roughness configuration.

The pre-activation roughness configuration, shown in Fig. 3, consisted of applying 40-grit silicon carbide (using double-sided tape) on both the wing and the tail protected and unprotected leading edges. The chord-wise extent of the roughness was determined using LEWICE.

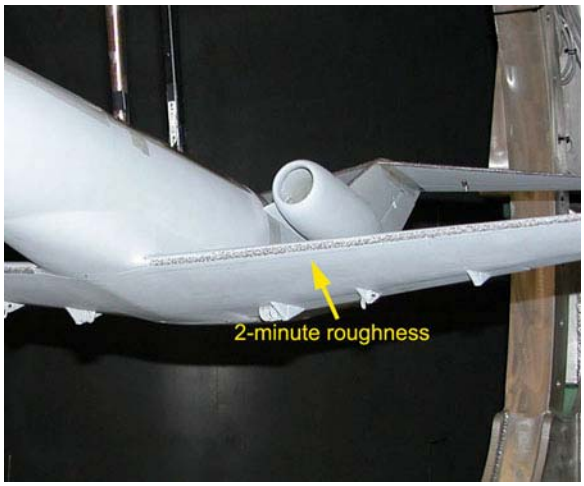

Figure 3. Pre-activation roughness configuration.

3. Runback ice shape configuration.

Instead of a geometrically scaled version of the full-scale runback shape, an aerodynamically equivalent shape (identified in a previous study) was used. It consisted of 0.025" diameter piano wire on the upper surface and 1/16" balsa square on the lower surface of the wing. These were located only on the protected surface of the wing. The unprotected surface of the wing and tail had the identical 45-minute LEWICE shape that was used in the failure shape configuration. The protected surface on the horizontal stabilizer was covered with 40-grit roughness to simulate inter-cycle ice (also identical to the failure-shape configuration). The wing upper surface of the runback configuration is shown in Fig. 4a, and the wing lower surface of the runback configuration is shown in Fig. 4b.

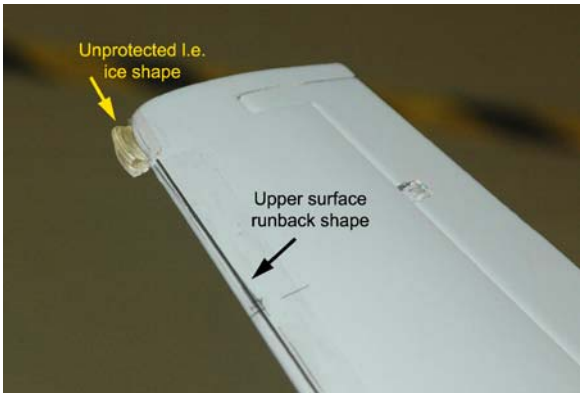

Fig. 4a) Wing upper surface.

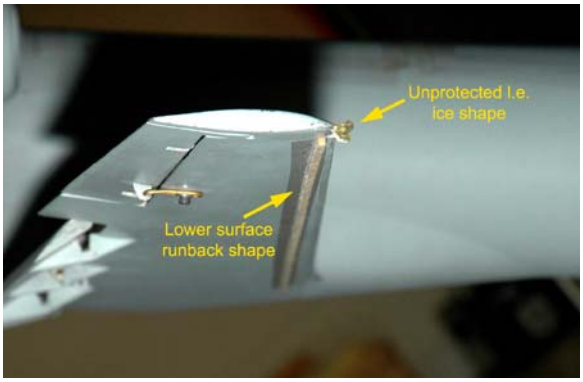

Fig. 4b) Wing lower surface.

Figure 4. Runback shape configuration.

III. Results and Discussion

An initial set of tests was run to look at the effect of dynamic pressure on the wind tunnel data. Static data were run at q_∞ = 1.0, 1.5, 2.0, and 3.0 psf. (The 3.0 psf case corresponded to the lowest speed tested during the scaling study and corresponded to a m.a.c. *Re* = 0.15 million.) Because there was essentially no difference between the 2.0 and 3.0 psf data, it was decided to run all of the data at 2.0 psf because the rotation rates and oscillatory frequencies at that speed were better within the facility's capability. Consequently, all of the test results for LAMP were run at q_∞ = 2.0 psf and corresponded to *Re* = 0.10 million.

The run program for this test was designed to provide the effects of angles of attack and sideslip, control deflections (elevator, aileron, rudder, and flaps), and icing configurations on the static and rotary aerodynamic characteristics, and on the forced oscillation data for oscillations about each body axis. Based on previous experience with this aircraft, and with other aircraft configurations, and on some preliminary test results, it was determined that not all control deflections were required for all of the dynamic (rotary and oscillatory) conditions. That is, it was determined that many control effects were essentially static. Consequently, the run program was limited to a more manageable level.

In the following plots, the absolute values of C_L, C_m, C_l, and angle of attack are not shown because the data were considered proprietary. However, the relative scales are shown in each plot.

1. Clean Configuration

Figures 5a and 5b show the comparison of the static lift coefficients measured at LAMP with those provided by the manufacturer (based on their low-speed wind tunnel data of q_∞ = 80 psf adjusted to flight determined C_{Lmax}) for neutral flaps and for flaps deflected, respectively. The lift characteristics measured in the LAMP wind tunnel are consistent with what would be expected at such low Reynolds numbers but, as shown, when shifted up to the C_{Lmax} from flight, provides a good simulation of the full-scale lift curve. For the simulation modeling, all of the other static and dynamic data (for the clean aircraft) would have to be similarly shifted to the flight stall angle of attack.

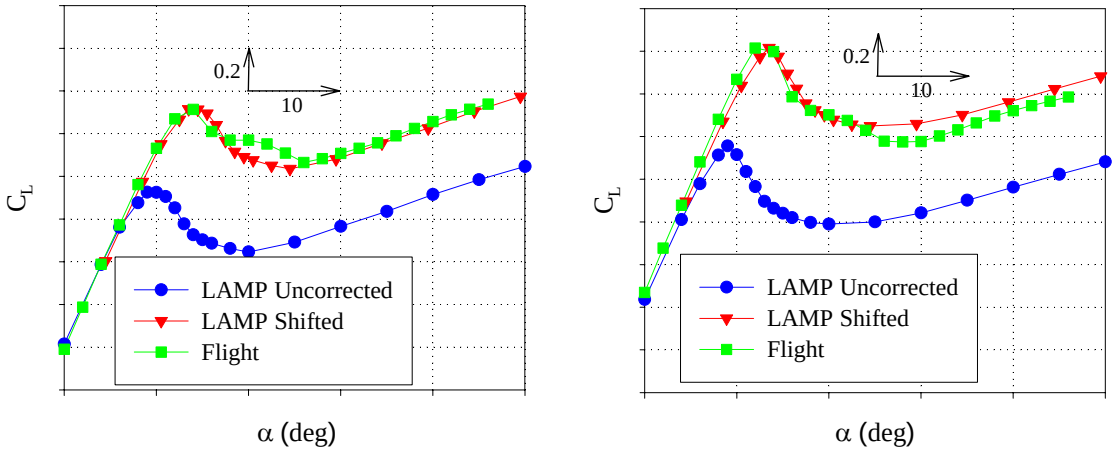

Fig. 5a) $\delta f = 0°$. **Fig. 5b) $\delta f = 20°$.**

Figure 5. Comparison of manufacturer's and LAMP lift coefficient data for $\delta f = 0$.

2. Ice Protection System Failure Configuration

The results of the ice protection system failure configuration on lift coefficient are shown in Fig. 6. The complete-aircraft results were from the LAMP facility (*Re* = 0.10 million) and the semi-span wing results were from the scaling study performed at the Langley Full Scale Tunnel (full-scale, *Re* = 4.1 million) and University of Illinois Subsonic Wind Tunnel (1/12-scale, *Re* = 0.15 million). The results show that for the complete aircraft (Fig. 6a), there was little change in maximum lift but a significant change in the post-stall lift characteristics. The stall process for the iced configuration was much more gradual than the clean configuration, with significantly higher lift values in the post stall region. There was also a slight decrease in the lift curve slope in the linear region. The semi-span wing results showed similar characteristics for the 1/12-scale model. The iced configuration showed reduced lift curve slope in the linear region, when compared to the clean configuration. However, this reduction was larger than what was observed for the complete aircraft. Another similarity was that the stall process for the iced configuration was more gradual than the clean configuration, with higher lift values in the post-stall region. However, the clean configuration exhibited significantly higher maximum lift. The full-scale semi-span model exhibited similar characteristics. However, the reduction in the maximum lift coefficient was much larger than with the 1/12-scale model because the clean maximum lift coefficient was much higher due to Reynolds number effect. The iced models did not exhibit significant Reynolds number effect.

The semi-span wing results showed substantially lower lift and lift curve slopes (when compared to the complete aircraft) because the lift coefficient for the 2/3 outer span of the wing was non-dimensionalized by the full semi-span area of the aircraft. As shown in Fig. 6b, the failure case was relatively insensitive to Reynolds number and geometric scaling effects, with the full-scale wing model at $Re = 4.1 \times 10^6$ having very similar characteristics to the 1/12-scale model at $Re = 0.15 \times 10^6$. Consequently, for the aero modeling of the clean airplane, data will be shifted to the flight stall angle, but the failure case data will require little or no shifting, resulting in the appropriate relative maximum lift and stall angle characteristics as the full-scale airplane.

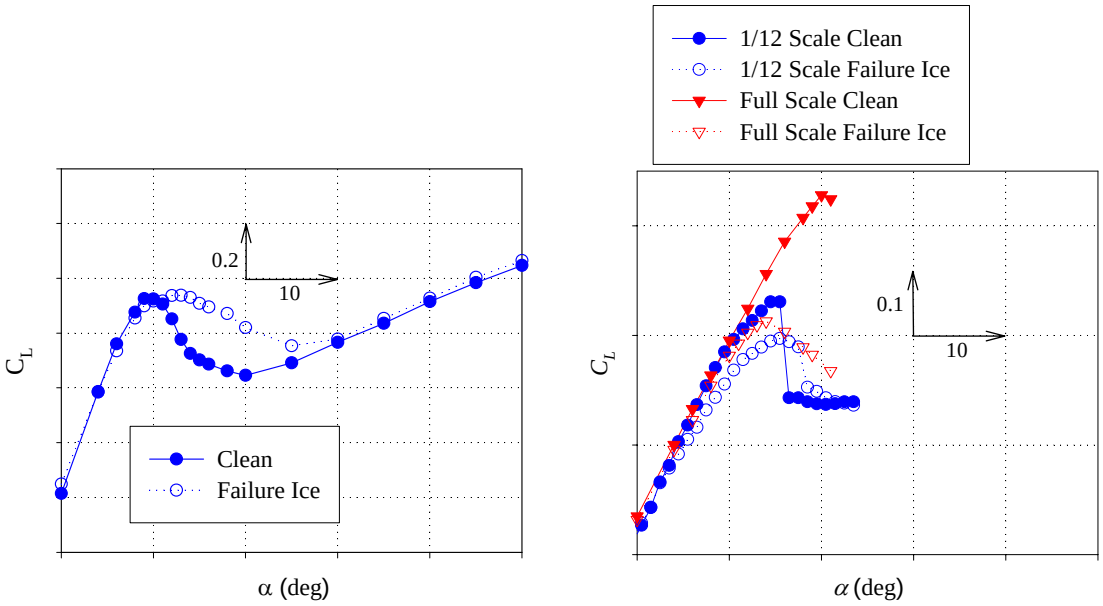

Fig. 6a) Complete aircraft **Fig. 6b) Semi-span wing**

Figure 6. Effect of ice protection system failure shape on lift coefficient.

3. Pre-Activation (Roughness) Ice Configuration

The influence of pre-activation roughness on the lift coefficient is shown in Figure 7. On the complete aircraft, the iced configuration resulted in significant reduction in the maximum lift. The lift curve slope in the linear region was significantly lower as well (much more so than for the failure configuration, Fig. 6a). The stall process was much more gradual for the iced configuration. Figure 7b shows that for the 1/12-scale semi-span wing, there was significant change in the maximum lift value and the lift curve slope in the linear region. The stall process for the iced configuration was more gradual as well. The full-scale wing also showed considerable differences between the clean and iced configurations. In fact, both the full scale and sub-scale iced configuration resulted in similar relative reduction in the lift coefficient when compared to the clean values.

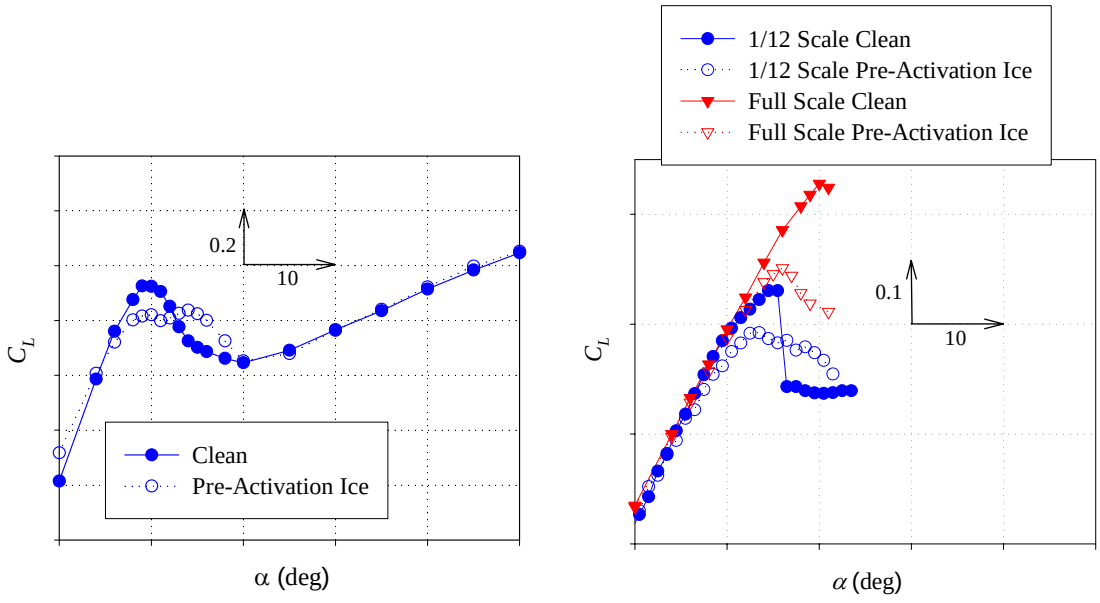

Fig. 7a) Complete aircraft **Fig. 7b) Semi-span wing**

Figure 7. Effect of pre-activation ice on lift coefficient.

4. Runback Ice

The effects of the runback ice configuration on the lift coefficient are shown in Fig. 8. On the complete aircraft, the runback ice configuration resulted in reduction of both maximum lift and lift curve slope. However, the stall angle of attack was not significantly affected. Also, in the post stall regions, the clean configuration lift coefficients were higher than those of the iced configuration. This was different from what was observed for the other two ice configurations. Similar results were observed for the semi-span wing. However, both the reduction in maximum lift and the lift curve slope were amplified. Significant Reynolds number effects were also observed for the iced configuration. Because of this, the runback iced configuration will require a shift in the maximum lift coefficient and the stall angle of attack when applied to the full-scale aircraft model.

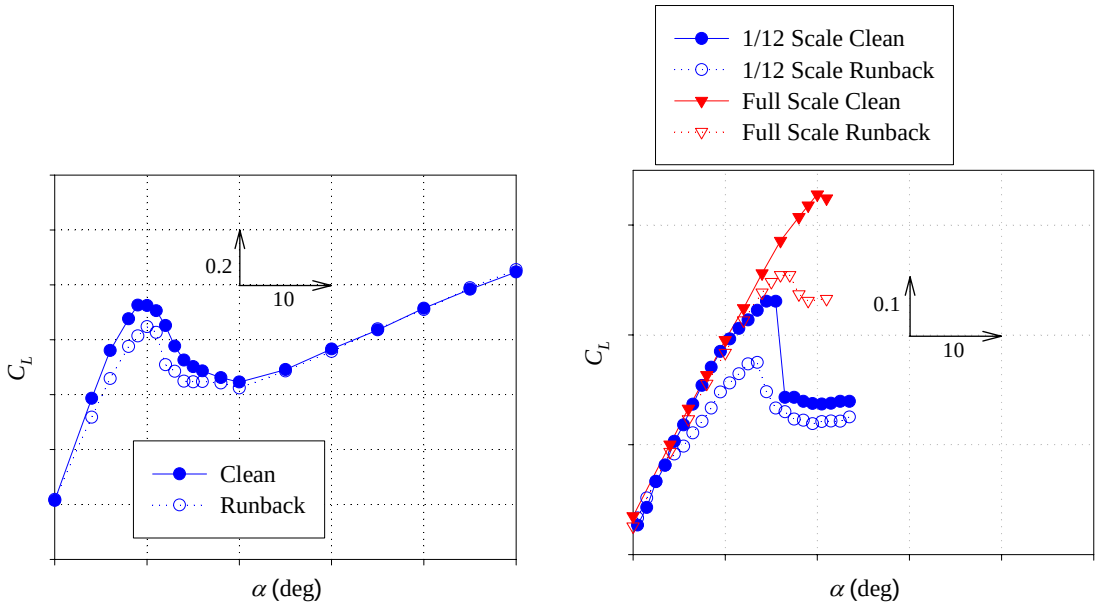

Fig. 8a) Complete aircraft **Fig. 8b) Semi-span wing**

Figure 8. Influence of runback ice on lift coefficient.

5. Flap Effects

The effects of the ice shapes on the flap effectiveness varied with the ice shapes tested. Figure 9a shows the clean aircraft with the flap deflected at 0, 20, and 40 degrees. It shows approximately a 0.2 increase in the C_L when the flap was deflected to 20 deg. However, when the flap was deflected further to 40 degrees, there was very little increase in the lift coefficient in the pre-stall region. This was likely due to the low Reynolds number of the test.

Figure 9b shows the effect of failure ice shape. As with the clean aircraft, lowering the flap to 20 deg increased the pre-stall lift coefficient by approximately 0.20. However, lowering the flap to 40 degrees resulted in slight further increase in the lift coefficient (approximately 0.05 in the pre-stall region) and increased the $C_{L,max}$ by 0.1. Similar results were observed for the pre-activation roughness and runback cases, as shown in Fig. 9c and Fig. 9d, respectively. Deploying the flap to 20 degrees resulted in 0.2 increase in pre-stall lift coefficient. Lowering the flap to 40 degrees resulted in a 0.05 increase in the pre-stall lift coefficient, and an increase in the maximum lift coefficient of approximately 0.1. Adding ice simulations on the leading edge of the wing may have enhanced boundary layer mixing and reduced the separation over the flap. In all cases, deploying the flap did not significantly alter the stall characteristics of the aircraft (when compared to zero flap deployment with the same iced configuration) and decreased the stall angle of attack by only 1 degree.

Figures 10a and 10b show the flap effectiveness with the various ice shapes at pre-stall and stall angles of attack. These figures show how at a fixed angle of attack, increasing the flap angle increases the lift coefficient. Figure 10a shows the flap effectiveness at a pre-stall angle of attack (same α for the clean and the three iced configuration). At the pre-stall angle of attack, deploying the flap to 20 degrees resulted in similar increases in lift coefficient for all of the cases. However, when the flap was increased to 40 degrees, there was no further increase for the clean aircraft. However, all three iced cases showed an increase in C_L of 0.1. Figure 10b shows the flap effectiveness at the stall angle of attack of the clean aircraft. The results were very similar to the pre-stall angle of attack.

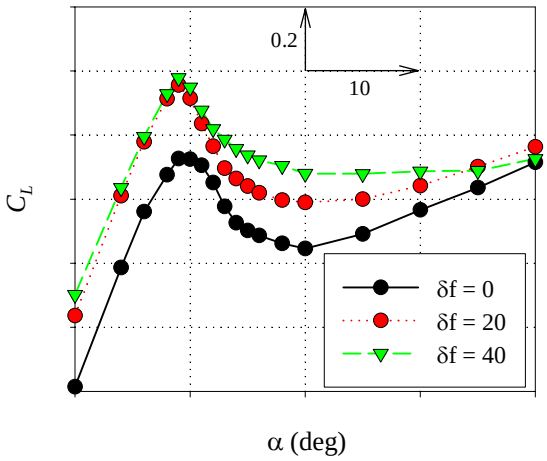

Fig. 9a) Clean config.

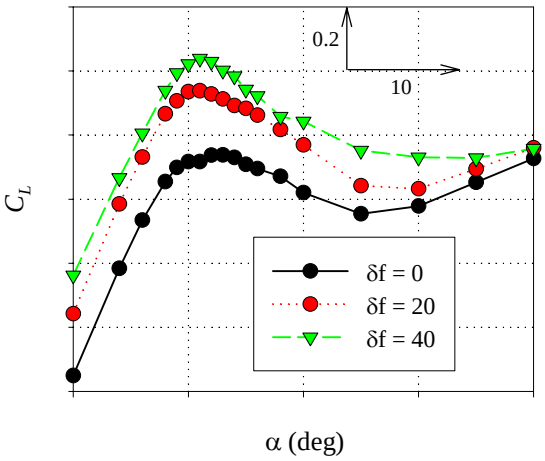

Fig. 9b) Failure config.

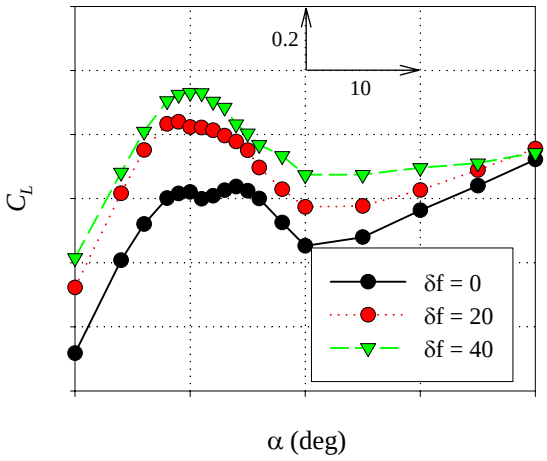

Fig. 9c) Pre-activation config.

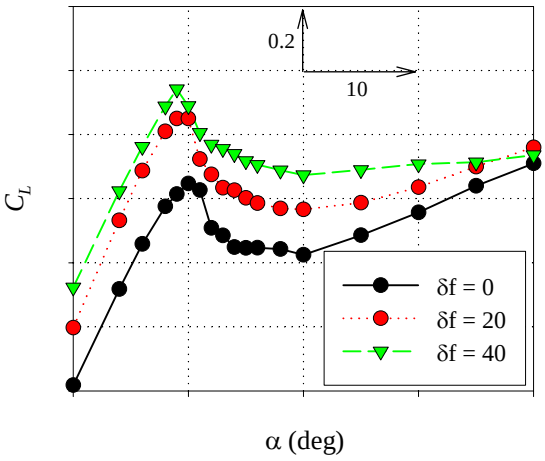

Fig. 9d) Runback config.

Figure 9. Effect of flap deployment on lift curve.

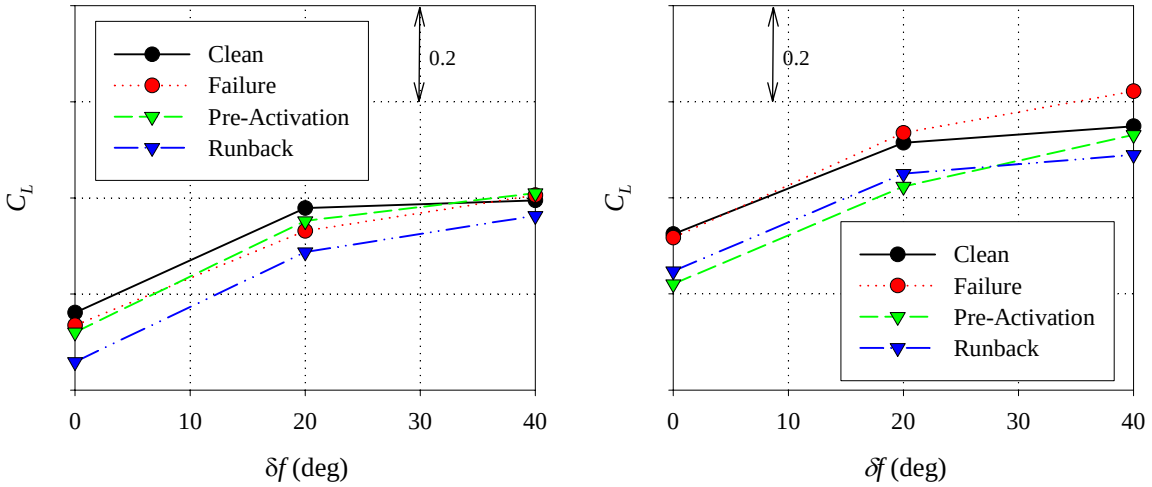

Fig. 10a) Pre-stall angle of attack **Fig. 10b) Stall angle of attack**

Figure 10. Effect of ice shapes on flap effectiveness.

6. Pitching Moment

Figure 11 shows the aircraft pitching moment with various ice configurations. It shows that at very low angles of attack, all of the iced configurations had more negative pitching moment. However, the failure and pre-activation roughness configurations resulted in a less aircraft nose-down pitching moment in the aircraft stall regions. The pitching moment with the runback shape matched the clean configuration closely in the stall region.

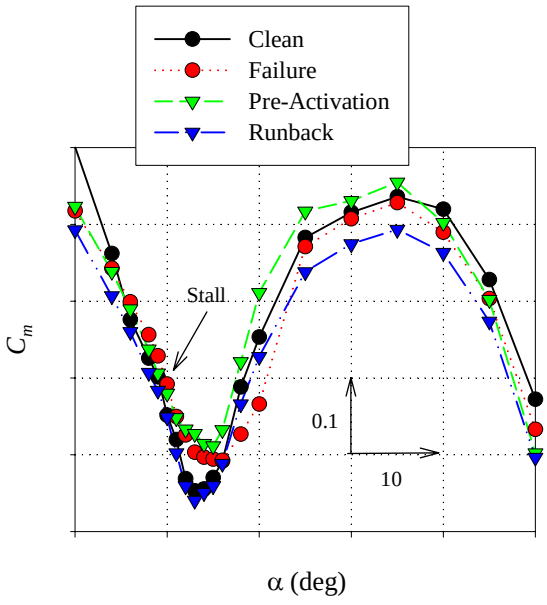

Figure 11. Pitching moment with various ice configurations.

Figure 12 shows the effect of ice shapes on the elevator effectiveness. The figure shows how, at a fixed angle of attack, varying the elevator deflection affects the aircraft pitching moment. Figure 12a shows that at the pre-stall angle of attack, there was a slight reduction in the elevator effectiveness for all three iced conditions, as shown by a slight decrease in C_m-δ*e* slopes. The reduction in the flap effectiveness was even more apparent at stall angle of attack (Fig. 12b). The reduction in the C_m-δ*e* slope of the iced configurations was more than twice that of the pre-

stall angle of attack. As with the pre-stall angle of attack, there was no iced case that clearly had less elevator effectiveness than the others. This was expected because as described in Sec. II, all of the iced configurations had essentially identical ice simulation (40-grit roughness).

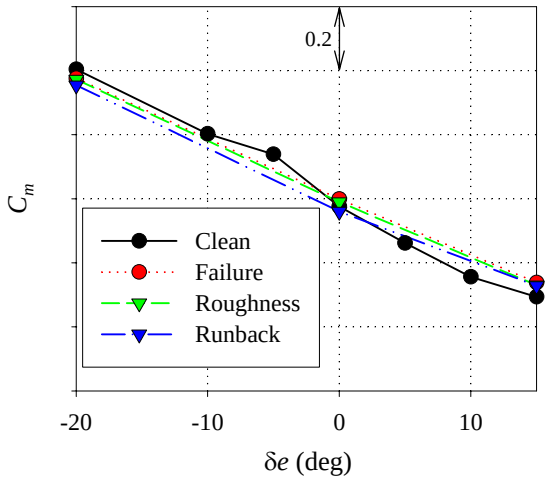

Fig. 12a) Pre-stall angle of attack

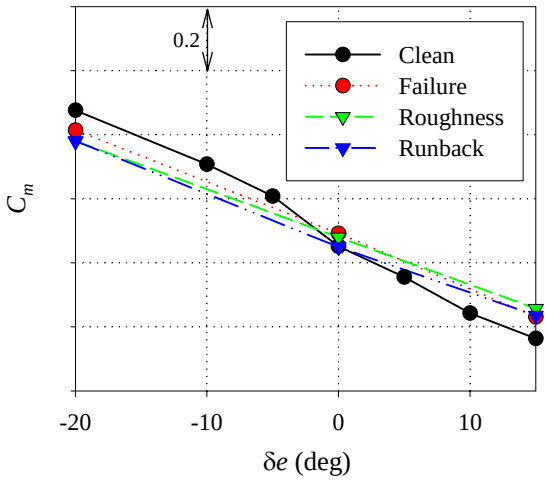

Fig. 12b) Stall angle of attack

Figure 12. Effect of ice shapes on elevator effectiveness.

7. Rotational Data

The effects of the icing on the rotational characteristics were virtually all seen in the stall region arising from the differences seen in their stall characteristics and their effects on the rotational rolling moment coefficient. Below stall, all were damped with little or no influence of the ice condition. In the stall region, the failure and pre-activation roughness ice conditions both flattened out the immediate post-stall lift curve, and, as a result, both have similar effects on the rotational roll characteristics. While the run-back ice condition produced a lower $C_{L,max}$, it produced nearly identical stall lift characteristics as were observed for the clean airplane and, as a result, the rotational rolling moments for the run-back are very similar to those of the clean airplane.

In the immediate post-stall region (Fig. 13a), the failure and pre-activation roughness ice conditions actually result in less propelling rolling moments than the clean or runback ice conditions do. At slightly higher angles of attack, however, the opposite effect is seen as they produce more propelling rolling moments (Figure 13b). At even higher angles of attack (Figure 13c), there is, again, no difference in the rotational characteristics due to the icing condition.

The effect of ice conditions on rotational yawing moment were generally seen in the same angle of attack region as roll, but were smaller and, at these angles of attack of less importance.

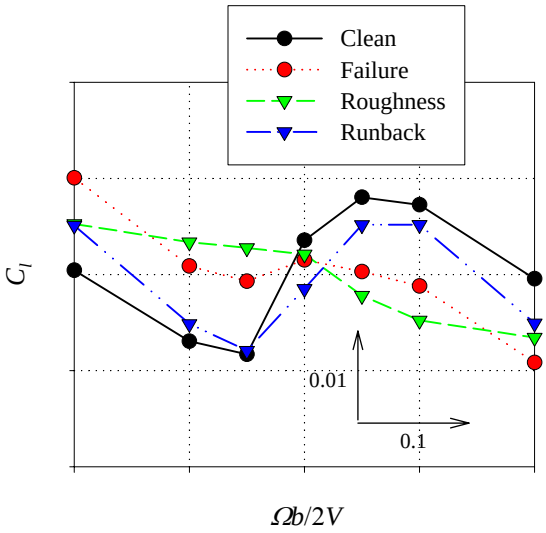

Fig. **13a) Immediate post stall angle of attack**

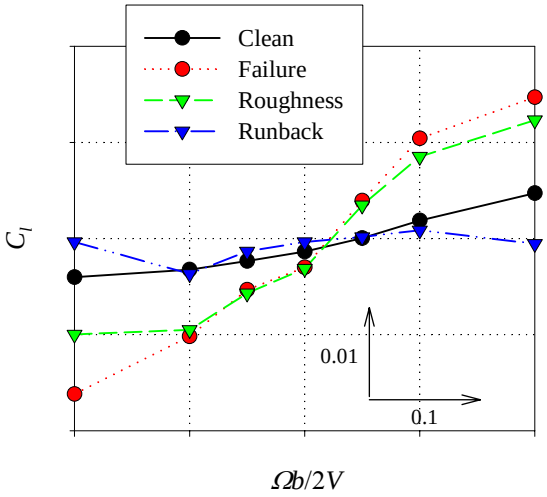

Fig. 13b) Post stall angle of attack

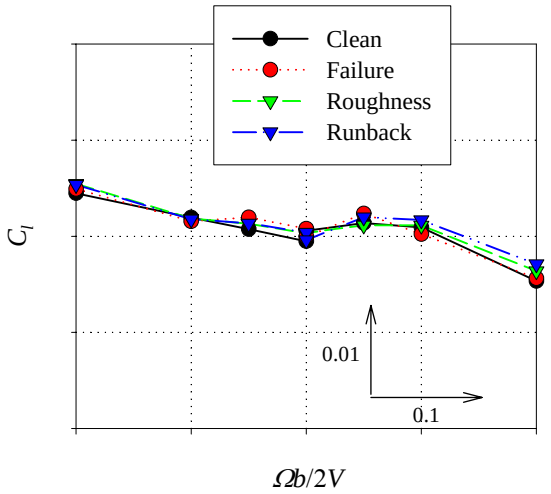

Fig. 13c) Significantly past stall angle of attack

Figure 13. Effect of ice on rotational rolling moment.

8. Forced Oscillation

Forced oscillation tests were performed about each body axis for the clean airplane and for each of the iced configurations. The influence of ice on the forced oscillation data was generally small and occurred mostly in the post-stall region, similar to the rotary effects.

The most apparent effect was on the rolling moment coefficient due to roll rate. In the normal flight regime all of the configurations are damped with only relatively minor differences due to the ice configuration, as shown in (Fig. 14a). The biggest differences in body-axis roll damping are seen in the immediate post-stall region (Fig. 14b) produced similarly to the differences seen in the rotary data. At higher angles of attack, all of the configurations exhibit identical characteristics. The yawing moment due to roll rate terms were not strongly influenced by the ice configuration beyond a small change in slope in the post-stall region.

The yawing moment due to yaw rate term shows little influence of ice configuration beyond a small increase in slope in the post-stall region for the failure and roughness conditions. A similar effect was seen in the rolling moment due to yaw rate term in the same angle of attack region. The ice configurations had very little effect on the pitch damping, except for a small region in the immediate post-stall region for positive pitch rates.

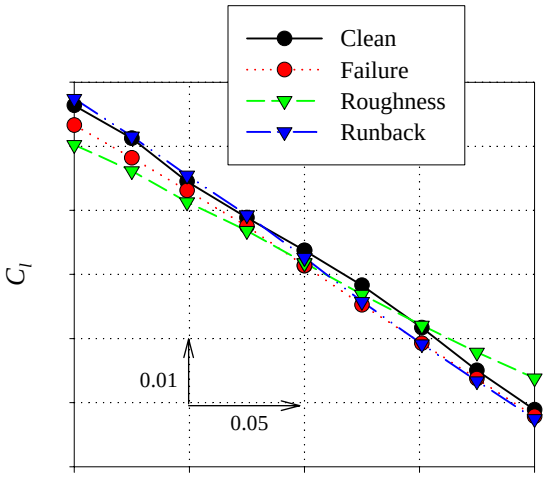

Fig. 14a) Pre-stall angle of attack

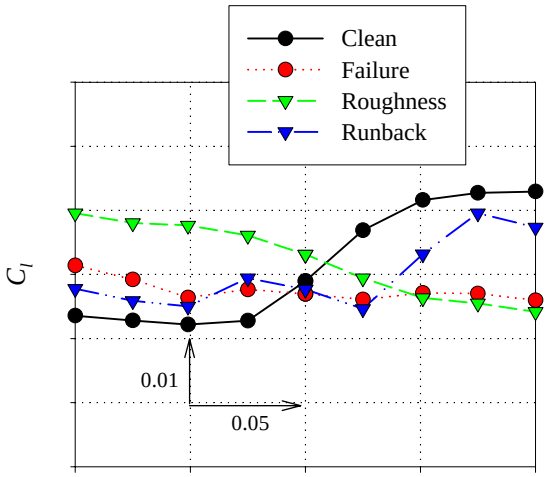

Fig. 14b) Immediate post stall angle of attack

Figure 14. Effect of ice and roll rate on rolling moment.

IV. Summary

Effects of ice accretion on a 1/12-scale complete aircraft model of a business jet were studied in a rotary-balance wind tunnel. Three types of ice accretions were considered: ice protection system failure shape, pre-activation roughness, and runback shapes that form downstream of the thermal ice-protection system. The results were compared with those from a 1/12-scale semi-span wing of the same aircraft at similar Reynolds number. The results showed that the full aircraft and the semi-span wing models showed similar characteristics, especially in the post stall behavior under iced configuration. However, there were also some discrepancies, such as reductions in the maximum lift coefficient.

There was a significant reduction in the clean-aircraft flap effectiveness at 40-degree flap extension due to Reynolds number effects. The ice accretions, however, did not appear to significantly affect the flap effectiveness. The ice shapes resulted in a more nose-down pitching moment at low angles of attack. In the stall regions, the failure and roughness configurations resulted in a less nose-down pitching moment. The runback configuration has pitching moment that was nearly identical to the clean configuration. All of the iced configurations showed reduced elevator effectiveness that worsened at stall angle of attack.

The effects of ice shapes on the rotational characteristics were not significant at pre-stall angles of attack. Most of the differences were observed in the stall and immediate post stall regions in the rolling moment. The effects of ice shapes on the rotational yawing moments were generally smaller. The most apparent effect of ice on the forced oscillation was measured in the rolling moment coefficient due to roll rate in the stall and immediate post-stall angles of attack. The ice configurations had little effect on pitch and yaw damping values.

References

[1]Gingras, D.R, Dickes, E.G, Ratvasky, T.P., and Barnhart, B.P, "Modeling of In-Flight Icing Effects for Pilot Training," AIAA Modeling and Simulation Technologies Conference and Exhibit, Aug. 5-8, 2002, Monterey, CA, AIAA Paper 2002-4605.

[2]Ratvasky, T.P, Ranaudo, R.J., Barnhart, B.P., Dickes, E.G, and Gingras, D.R, "Development and Utility of a Piloted Flight Simulator for Icing Effects Training," AIAA 41st Aerospace Sciences Meeting and Exhibit, Jan. 6-9, 2003, Reno, NV, AIAA Paper 2003-0022.

[3]Papadakis, M., Gile Laflin, B.E., Youssef, G.M, and Ratvasky, T.P., "Aerodynamic Scaling Experiments with Simulated Ice Accretions," AIAA 39th Aerospace Sciences Meeting and Exhibits, Jan. 8-11, 2001, Reno, NV, AIAA Paper 2001-0833.

[4]Lee,S., Ratvasky, T.P., Thacker,M., and Barnhart, B.P., "Geometry and Reynolds Number on an Iced Business Jet Wing," AIAA 43rd Aerospace Sciences Meeting and Exhibits, Jan. 10-13, 2005, Reno, NV, AIAA Paper 2005-1066.

[5]Wright, W.B., User Manual for the NASA Glenn Ice Accretion Code LEWIC, NASA CR 2002-211793, Aug. 2002.

REPORT DOCUMENTATION PAGE

Form Approved
OMB No. 0704-0188

1. AGENCY USE ONLY (*Leave blank*)	2. REPORT DATE	3. REPORT TYPE AND DATES COVERED
	May 2006	Technical Memorandum

4. TITLE AND SUBTITLE

Dynamic Wind-Tunnel Testing of a Sub-Scale Iced Business Jet

5. FUNDING NUMBERS

WBS–457280.02.07.03.02

6. AUTHOR(S)

Sam Lee, Billy P. Barnhart, Thomas P. Ratvasky, Edward Dickes, and Michael Thacker

7. PERFORMING ORGANIZATION NAME(S) AND ADDRESS(ES)

National Aeronautics and Space Administration
John H. Glenn Research Center at Lewis Field
Cleveland, Ohio 44135–3191

8. PERFORMING ORGANIZATION REPORT NUMBER

E–15554

9. SPONSORING/MONITORING AGENCY NAME(S) AND ADDRESS(ES)

National Aeronautics and Space Administration
Washington, DC 20546–0001

10. SPONSORING/MONITORING AGENCY REPORT NUMBER

NASA TM—2006-214268
AIAA–2006–0261

11. SUPPLEMENTARY NOTES

Prepared for the 44th Aerospace Sciences Meeting and Exhibit sponsored by the American Institute of Aeronautics and Astronautics, Reno, Nevada, January 9–12, 2006. Sam Lee, QSS Group, Inc., 21000 Brookpark Road, Cleveland, Ohio, 44135; Billy P. Barnhart and Edward Dickes, Bihrle Applied Research, Inc., 400 Jericho Turnpike, Suite 216, Jericho, New York, 11753; Thomas P. Ratvasky, NASA Glenn Research Center, Cleveland, Ohio; and Michael Thacker, Cessna Aircraft Company, Wichita, Kansas 67218. Responsible person, Sam Lee, organization code RTI, 216–433–5296.

12a. DISTRIBUTION/AVAILABILITY STATEMENT

Unclassified - Unlimited
Subject Category: 05

Available electronically at http://gltrs.grc.nasa.gov

This publication is available from the NASA Center for AeroSpace Information, 301–621–0390.

12b. DISTRIBUTION CODE

13. ABSTRACT ***(Maximum 200 words)***

The effect of ice accretion on a 1/12-scale complete aircraft model of a business jet was studied in a rotary-balance wind tunnel. Three types of ice accretions were considered: ice protection system failure shape, pre-activation roughness, and runback shapes that form downstream of the thermal ice protection system. The results were compared with those from a 1/12-scale semi-span wing of the same aircraft at similar Reynolds number. The data showed that the full aircraft and the semi-span wing models showed similar characteristics, especially post stall behavior under iced configuration. However, there were also some discrepancies, such as the magnitude in the reductions in the maximum lift coefficient. Most of the ice-induced effects were limited to longitudinal forces. Rotational and forced oscillation studies showed that the effects of ice on lateral forces were relatively minor.

14. SUBJECT TERMS	15. NUMBER OF PAGES
Aircraft icing; Scaling; Aerodynamic stalling	20
	16. PRICE CODE

17. SECURITY CLASSIFICATION OF REPORT	18. SECURITY CLASSIFICATION OF THIS PAGE	19. SECURITY CLASSIFICATION OF ABSTRACT	20. LIMITATION OF ABSTRACT
Unclassified	Unclassified	Unclassified	